SAND REPORT

SAND2004-6435
Unlimited Release
Printed December 2004

Extraordinary Optical Transmission through Patterned Subwavelength Apertures

David W. Peters, Ihab El-Kady, Shanalyn A. Kemme, G. Ronald Hadley, and Chris E. Lanes

Prepared by
Sandia National Laboratories
Albuquerque, New Mexico 87185 and Livermore, California 94550

Sandia is a multiprogram laboratory operated by Sandia Corporation, a Lockheed Martin Company, for the United States Department of Energy's National Nuclear Security Administration under Contract DE-AC04-94-AL85000.

Issued by Sandia National Laboratories, operated for the United States Department of Energy by Sandia Corporation.

Available to DOE and DOE contractors from
U.S. Department of Energy
Office of Scientific and Technical Information
P.O. Box 62
Oak Ridge, TN 37831

Telephone: (865)576-8401
Facsimile: (865)576-5728
E-Mail: reports@adonis.osti.gov
Online ordering: http://www.doe.gov/bridge

Available to the public from
U.S. Department of Commerce
National Technical Information Service
5285 Port Royal Rd
Springfield, VA 22161

Telephone: (800)553-6847
Facsimile: (703)605-6900
E-Mail: orders@ntis.fedworld.gov
Online order: http://www.ntis.gov/help/ordermethods.asp?loc=7-4-0#online

SAND 2004-6435
Unlimited Release
Printed December 2004

Extraordinary Optical Transmission through Patterned Subwavelength Apertures
LDRD 67105 Final Report

David W. Peters, Ihab El-Kady, Shanalyn A. Kemme
Photonic Microsystems Technologies

G. Ronald Hadley
RF Microsystems Technologies

Chris E. Lanes
Satellite Systems Engineering

Sandia National Laboratories
P.O. Box 5800 M/S 0603
Albuquerque, NM 87185-0603

Abstract

Light propagating through a subwavelength aperture can be dramatically increased by etching a grating in the metal around the hole. Moreover, light that would typically broadly diverge when passing through an unpatterned subwavelength hole can be directed into a narrow beam by utilizing a specific pattern around the aperture. While the increased transmission and narrowed angular emission appear to defy far-field diffraction theory, they are consistent with a fortuitous plasmon/photon coupling. In addition, the coupling between photons and surface plasmons affects the emissivity of a surface comprised of such structures.

These properties are useful across several strategic areas of interest to Sandia. A controllable emission spectrum could benefit satellite and military application areas. Photolithography and near-field microscopy are natural applications for a system that controls light beyond the diffraction limit in a manner that is easily parallelizable.

Over the one year of this LDRD, we have built or modified the numerical tools necessary to model such structures. These numerical codes and the knowledge base for using them appropriately will be available in the future for modeling work on surface plasmons or other optical modeling at Sandia. Using these tools, we have designed and optimized structures for various transmission or emission properties. We demonstrate the ability to design a metallic skin with an emissivity peak at a pre-determined wavelength in the spectrum. We optimize structures for maximum light transmission and show transmitted beams that beat the far-field diffraction limit.

This Page Intentionally Left Blank

Table of Contents

This Page Intentionally Left Blank

Motivation

Surface plasmon interaction with free-space modes offers interesting capabilities for controlling the transmission and emission of light from metallic surfaces. We demonstrate numerical methods for designing structures with specific transmission or emission requirements. The ability to optimize structures with fast numerical methods allows for more productive use of fabrication facilities. The ability to model the emission opens new areas of application for metallic skins employing surface plasmon interactions.

Surface plasmons have been shown to greatly enhance the transmission through an aperture when a grating is patterned in the adjacent metal. This grating allows coupling to surface plasmon modes at the metal/air interface. These surface plasmon modes in turn recouple to radiating modes on the other side of the aperture. Although the apertures are well under a wavelength in scale, a sizable fraction of light will transmit through as a result of the surface plasmon interaction. In addition, the divergence of the exiting beam is significantly lower than would be expected from diffraction theory. We further explore this transmission coupled with a study of absorption and emission from a surface covered in such apertures. A representative, but in no way comprehensive, reference list is [1-5]. This controlled beaming of very small low-divergence beams is applicable to photolithography, near-field microscopy, and optical tweezers for holding small biological or other particles.

Surface Plasmons Background

Surface plasmons are electromagnetic waveforms that can be fully described using Maxwell's equations. Surface plasmons are modes of the surface charge density at an interface. Coherent fluctuations of electrons at a metal/dielectric boundary lead to electromagnetic fields whose strength drops exponentially in both directions from the surface as shown in Fig. 1. The existence of surface plasmons is dependent on one dielectric constant at the interface having a negative real component, and the other dielectric constant being positive. For this reason, surface plasmons can exist only at interfaces of a dielectric and either a metal or highly-doped semiconductor.

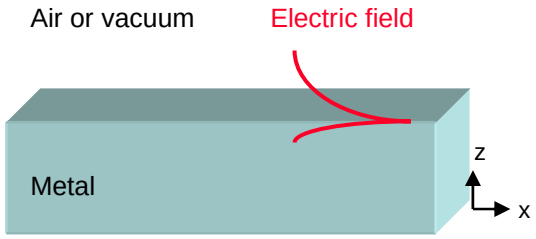

Fig. 1. Surface plasmon electric field distribution at a metal/air interface.

The wave vector for surface plasmons is always greater than the photon wave vector. Therefore, coupling directly from photons to surface plasmons on an idealized flat surface is impossible. However, structuring the surface in the form of a grating can match the wave vectors to accomplish this coupling. The exponential decay away from the interface makes surface plasmons sensitive to surface properties. This property is fortuitous in that relatively shallow surface-relief gratings can couple propagating plane waves to surface plasmons efficiently.

A surface-relief grating is a simple corrugation on the surface. A one-dimensional grating (linear grooves) has a distinct restriction when working with surface plasmon/photon interaction. Interaction between surface plasmons only occurs with photons where the electric field is perpendicular to the direction of the grating corrugation. A two-dimensional grating overcomes this restriction, allowing coupling into both polarization states.

A sample one-dimensional surface-relief grating in a metal is illustrated in Fig. 2.

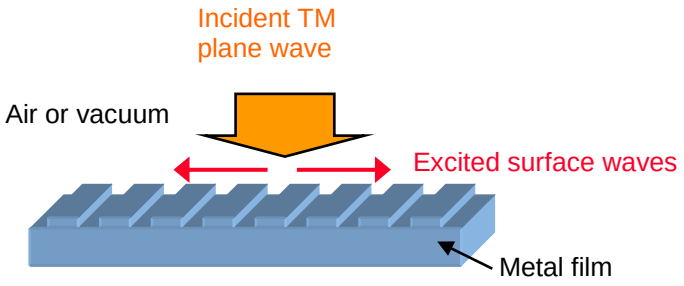

Fig. 2. Coupling from a free-space propagating wave to a surface wave by means of a grating.

A grating with a fixed period will couple light of a particular frequency into a surface plasmon. To the observer this will appear as a dip in the reflectance at particular wavelengths and angles. This dip represents photons being converted to surface plasmons, and the consequent absorption of the surface plasmon energy into the surface.

Kirchhoff's Law states that the absorptivity is equal to the emissivity under conditions of thermal equilibrium. The law applies to the spectral absorptivity and emissivity, or the integrated values over the same spectral band, or each component of the polarization. This means that the spectral locations where photons are absorbed correspond to wavelengths where emission will occur if the surface is heated. Surface plasmons may thus be used to produce emission peaks at desired wavelengths by tailoring the grating specifications.

An extension from the corrugated surface is the metal film with a slit through it as shown in Fig. 3. The surface waves may now travel on the metal surface through the aperture and recouple to a propagating wave on the back surface with the aid of the surface-relief grating on the back side.

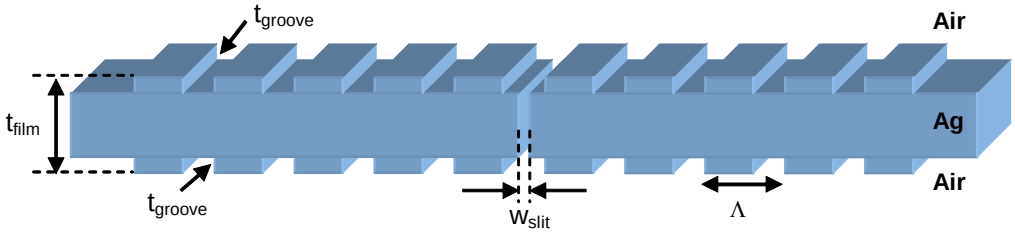

Fig. 3. Test structure for transmission and emission numerical study.

We theoretically modeled this structure, which consists of a silver film of thickness t_{film} in which parallel grooves are etched to a depth t_{groove} on both faces about a central slit of width w_{slit}. The

parallel grooves can be viewed as constituting a one-dimensional lattice of lattice constant Λ. The corresponding reciprocal lattice vector is,

$$\vec{G}_1 = \frac{2\pi}{\Lambda}\hat{x} \tag{1}$$

Such periodic metal films have longitudinal surface plasmon modes propagating along the surface (with an **E** field and charge oscillation along the propagation direction), and an exponentially decaying amplitude perpendicular to the interface. The surface plasmon dispersion relation [6] is given by

$$k_{sp} = \frac{\omega}{c}\left[\frac{\varepsilon_1\varepsilon_2}{\varepsilon_1+\varepsilon_2}\right]^{\frac{1}{2}}. \tag{2}$$

(1)

ε_2 is the real part of the metallic dielectric function, which is negative and large in magnitude for IR frequencies. ε_1 describes the response of the dielectric media. Since the surface plasmon dispersion lies below the incoming light line for any angle of incidence (θ, measured from the normal), incoming light cannot directly generate surface plasmons on a smooth surface. When an incident light beam of frequency ω, impinges on the patterned surface at an angle θ, it can couple to a surface plasmon at the air/metal interface through a surface reciprocal lattice vector [2,7]:

$$\frac{\omega}{c}\sin\theta\,\hat{\mathbf{n}} + \mathbf{G} = \mathbf{k}_{sp} \tag{3}$$

(2)

Where $\hat{\mathbf{n}}$ is a unit vector lying in the plane of incidence, and θ is the angle of incidence with respect to the normal to the surface of the crystal assumed here to be the xy-plane. By combining the dispersion relation (1) with this momentum conservation condition (2), we obtain the following eigenvalue equation for the surface plasmon frequencies

$$\left[\frac{\varepsilon_1\varepsilon_2}{\varepsilon_1+\varepsilon_2}\right] = \left[\sin\theta\cos\phi \pm i\frac{\nu_0}{\nu}\right]^2 + \left[\sin\theta\sin\phi\right]^2 \tag{4}$$

Here ν is the surface plasmon frequency, i is an integer, ϕ is the azimuthal angle, and $\nu_o = c / \Lambda$. The fundamental surface plasmon mode ($i=1$, corresponding to the first shell of G vectors) occurs at a wavelength of Λ. The strength of higher order surface plasmon modes is expected to decrease rapidly beyond the fundamental mode.

Modeling Methods

The numerical results shown here have been generated using three numerical simulation tools. The use of multiple modeling methods allows verification of results from one code to another. Moreover, some codes are better suited to certain aspects of a particular problem. We used rigorous coupled wave analysis, a semi-vectorial finite-difference Helmholtz code, and a transfer matrix method code.

Rigorous coupled wave analysis (RCWA) gives the far-field reflectivity and transmission from a periodic structure, with periodicity in either one or two dimensions. Absorption may then be calculated given reflection and transmission. Non-periodic structures such as the slit of Fig. 3 may be modeled if the entire structure is repeated periodically. RCWA is a fast simulation tool, however difficulties with numerical stability can be encountered with metallic structures with TM excitation, the case of interest here. Overcoming the stability issue can slow the code considerably, however it is still the fastest method used here and was often used to obtain rough results before employing another method.

We also use the well established transfer matrix method (TMM) for solving Maxwell's equations. Here harmonic time dependence is assumed for the impinging electromagnetic waves. This renders the time derivatives of Maxwell's equations, a simple frequency multiplicative factor. Space is then discretized, and the spatial derivatives are cast into a set of finite difference equations that allow us to track the fields as they are stepped forward in numerical space. One field component, specifically the one marking the direction of the fields progression in the structure (usually chosen to be the Z-component), is then eliminated in favor of the other two. In the end the resulting equations are cast in matrix form, where the electromagnetic tensor on the exit face of the structure is given as the product of a transfer matrix, and the field tensor at the entrance face of the structure. As is easily inferred, the transfer matrix is dependent only on the optical properties of the medium under study. Reflection and transmission coefficient information is then easily extracted from this transfer matrix by subjecting it to the appropriate boundary conditions.

The third code discretizes the space and using a finite-difference semivectorial Helmholtz equation-based formulation. This code allows us to see the fields present in the structure. This feature allows us to gain insight into the physics of what is happening inside the structure, thus leading to increased understanding and better design. For over ten years, numerical simulation of electromagnetic fields in two-dimensional structures that generate reflections has been accomplished by solving the semivectorial Helmholtz equation using a finite difference method [8,9]. The adjective "semivectorial" refers to the fact that, although only a single field component is computed, correct interface conditions are maintained at dielectric interfaces, resulting in accurate solutions for two-dimensional geometries. As a result, the solution is different depending on whether the single field component is E or H, i.e. polarization effects may be examined. This finite difference method has been coded into a highly-accurate computer program (SHIM, for Semivectorial Helmholtz solution by an Iterative Method) that allows variable zoning in both directions and has a fourth-order spatial truncation error. This code has been successfully employed for the simulation of a wide variety of photonic structures such as binary focusing lenses, spatial light modulators, and second-order gratings, to name just a few.

Until recently, all these structures were either polarization insensitive, or were amenable to modeling with TE polarization (the computed field is the out-of-the-plane component of E). Code had not been generated for the other polarization because of the complexity of the derivation required (see, for example, ref. [9]). However, the present investigation of transmission through metallic sub-wavelength apertures was only possible with TM polarization due to the inability of TE-polarized waves to couple to surface plasmon modes and thus a high extinction of the TE-polarized wave as it passes through the aperture. Consequently, the equivalent fourth-order

derivation for TM polarization was performed and included in the code, resulting in a numerical tool which now can model either polarization.

RCWA modeling of grating

Surface plasmon resonances and their relative strengths can be determined by modeling the periodic grating without the aperture. This simplifies the problem numerically and can be modeled quickly using RCWA. Two-dimensional plots where two parameters are varied are possible with RCWA since the time for an individual simulation is fast.

In Fig. 4 we see a plot that demonstrates some of the issues involved with designing such surfaces. The absorptivity of a gold film is plotted as a function of wavelength and grating depth. The surface wave absorptivity is seen as a strong peak between 0.5 and 0.6μm. However, a strong material absorption from the gold is seen immediately adjacent to the absorption caused by the designed grating. This illustrates the problematic nature of gold in the visible wavelength range; this material absorptivity cannot be altered by the structure and necessitates the need to use silver films for the visible. However, the rapid oxidation of unprotected silver makes it non-optimal for many applications. Luckily, gold is an acceptable solution for applications in wavelength bands from the mid-visible to longer wavelengths.

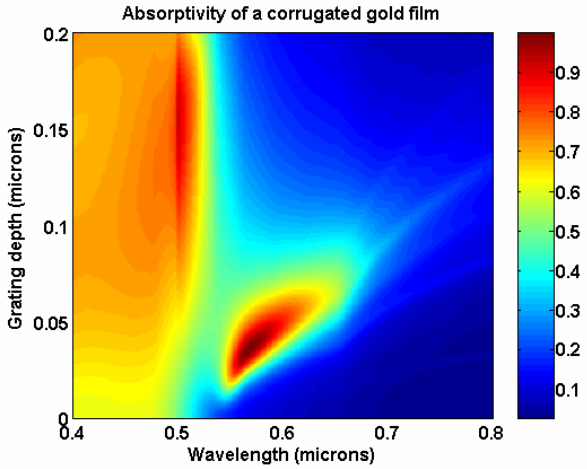

Fig. 4. Absorptivity (emissivity) of a gold film with Λ = 0.5μm grating.

The angular dependence of the absorptivity of the surface (and thus the emissivity) can be seen in Fig. 5. The dotted nature of the gold graph is a result of the discretization used in the simulation, if a finer discretization were used a solid thin line would be seen. From these graphs we can see that a strong emissivity peak can be designed at a given wavelength and angle.

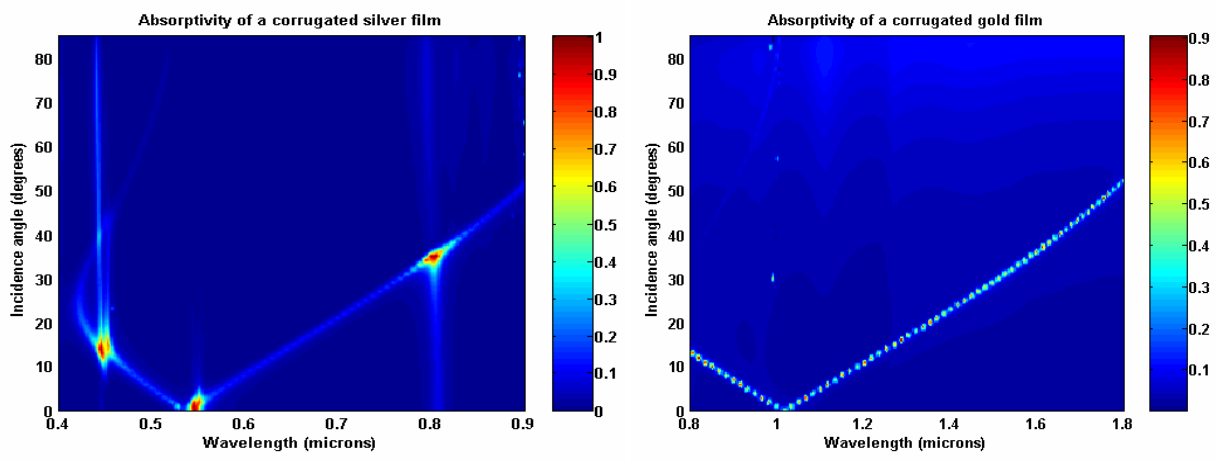

Fig. 5. Absorptivity (emissivity) of a silver film with etched grating (Λ = 0.5μm) and a gold film in the near IR (Λ = 1.0μm) as a function of wavelength and angle.

Transmission through slit

We modeled the structure published by Lezec, et al.[4] We then varied the parameters of this structure in silver film to maximize the coupling of light through the aperture. The basic structure is shown in Fig. 3. By varying the aperture width, film thickness, and grating depth we determined the optimal structure for transmission.

Numerical modeling for transmission is performed using the modified semi-vectorial Helmholtz code described in the previous section. This high-order accurate code does not require the density of grid points that a second-order accurate code would require. For modeling metallic structures such as these, the lowered grid point requirement allows for larger structures to be simulated. A typical field pattern is shown in Fig. 6. Sinusoidally-increasing absorbing boundary conditions are used at simulation boundaries. Far-field patterns of the exiting beam are determined by taking the Fourier transform of the exiting field at the top row of grid points before the top absorbing boundary. The input beam is a Gaussian with a FWHM of 4μm. This width is considerably wider than the size of the aperture. Strong fields can be observed at the silver/air interface that decay exponentially into the air and silver layers.

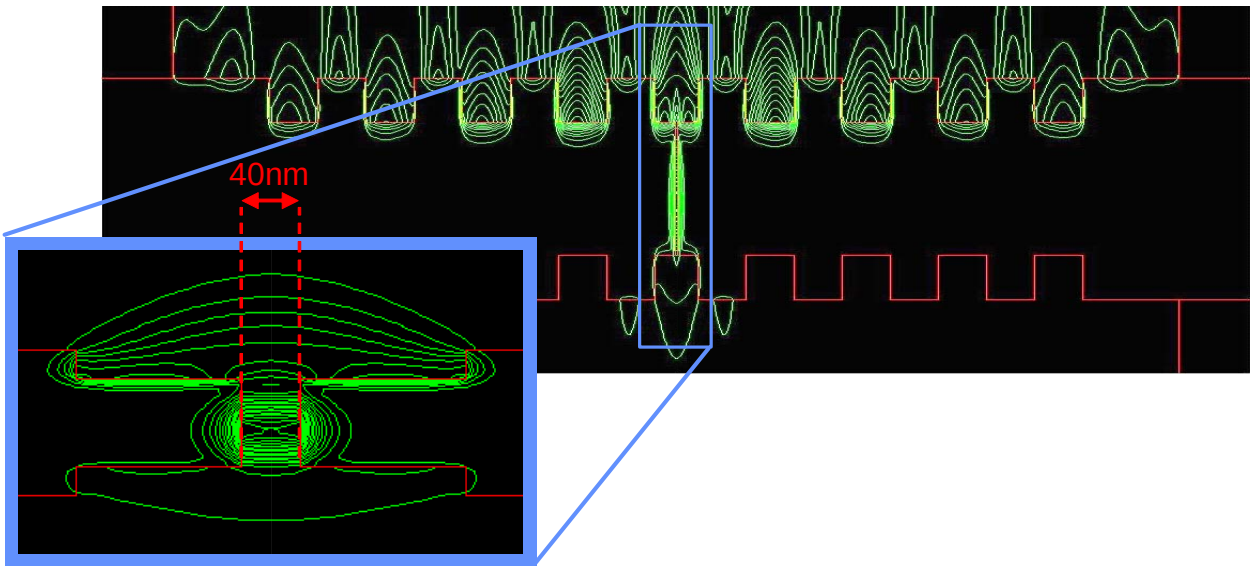

Fig. 6. TM mode transmittance through a 40nm aperture in a patterned gold film from Helmholtz equation code.

The fields shown here are for a 40nm slit width. Strong coupling of the evanescent fields can be seen across the gap of the slit. The exiting light on the back side of the metal film (bottom side in figure) can also be seen.

Light transmitted through the aperture is a function of the slit width. As the slit width is narrowed below the 40nm width, the light transmitted falls off precipitously as seen in the peaks in the spectral plot of Fig. 7. The 60nm slit-width curve corresponds well to Lezec's published experimental results.

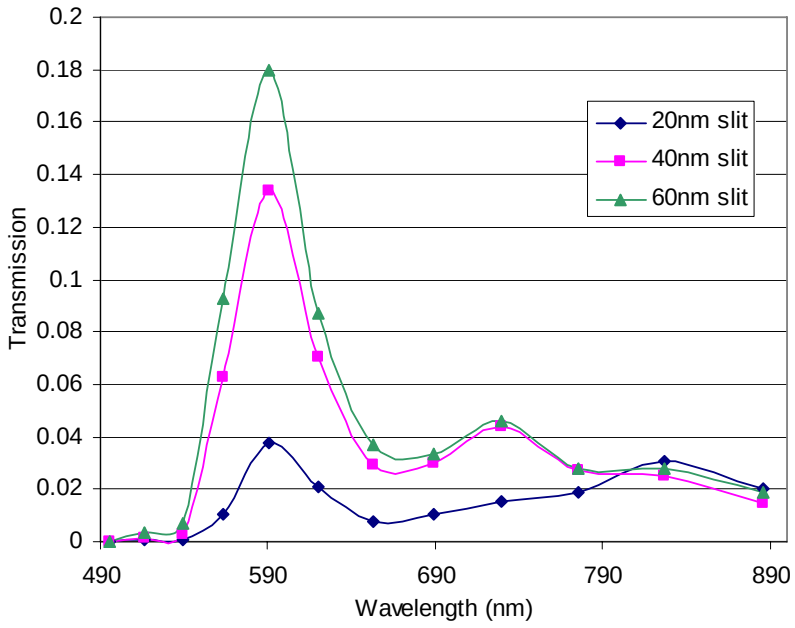

Fig. 7. Transmission of a 4μm normally-incident Gaussian through patterned aperture with varying slit widths.

The far-field patterns of these three slit widths were also calculated. The other parameters of the structure are identical for the three. The resulting angular spread is shown in Fig. 8. It is clear that the slit width does not affect the far-field angular distribution. Note that for a slit width that is much smaller than an incident wavelength (and in the 20nm case around 1/30 of the wavelength) the angular divergence half-angle is under 10 degrees.

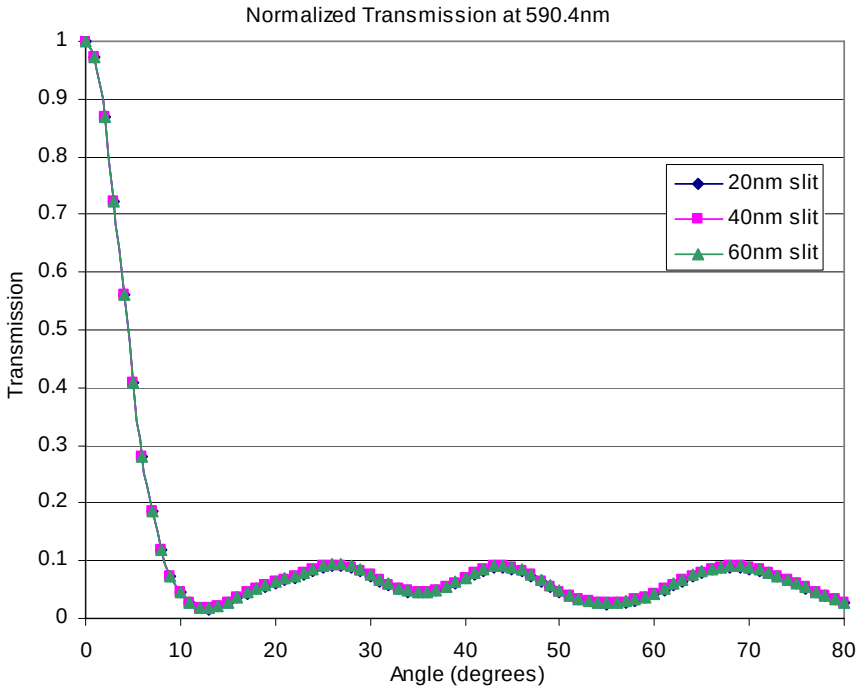

Fig. 8. Angular distribution of power in the far-field for three slit widths.

It is tempting to continue increasing the slit width to increase transmission, particularly since it will not affect the angular divergence of the transmitted beam. However, the slit cannot be expanded indefinitely with the expectation that the transmitted power will continue to rise monotonically. The reason for an eventual drop in the transmitted power, even with a wider slit, can be seen in Fig. 9. The exponential decay of the field between the two sides of the slit is apparent in the expanded detail of the fields in the slit region. As the slit width increases past 100nm the transmission continues to fall; the transmission as a function of slit width is shown in Fig. 10. These data were for a wavelength of 590.4nm (near the transmission peak).

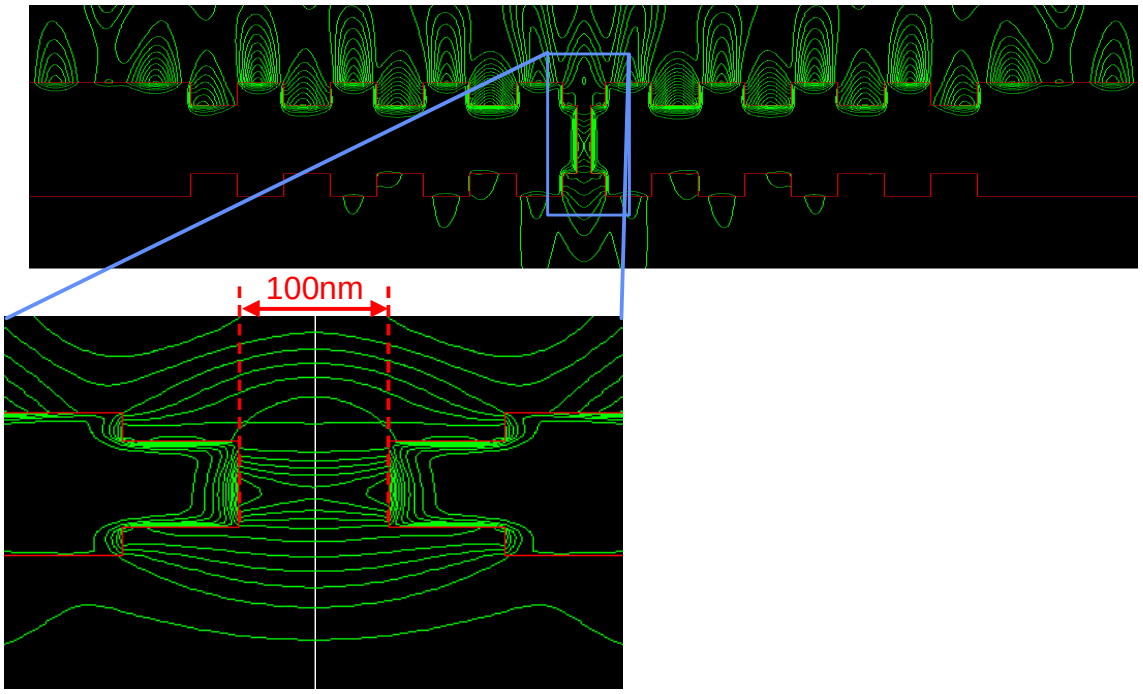

Fig. 9. TM mode transmittance through a 100nm aperture in a patterned gold film from Helmholtz equation code.

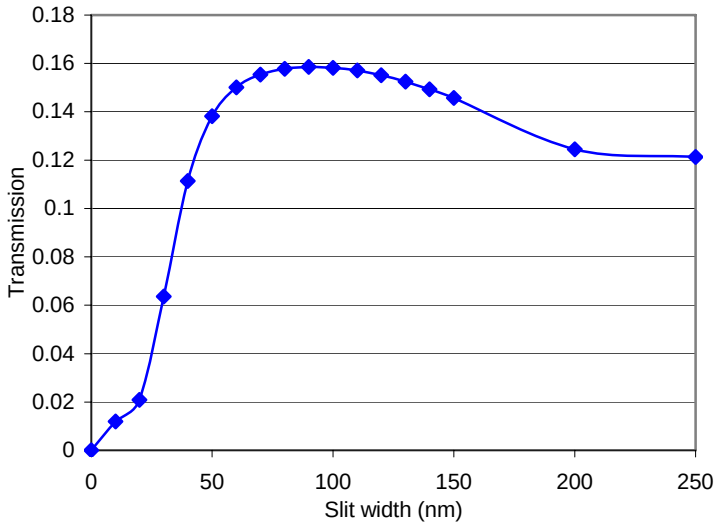

Fig. 10. Transmission of 4μm wide Gaussian through slit in linearly-patterned silver 300nm thick film with dual-sided 60nm-deep gratings as a function of slit width.

A variation of the thickness of the metal film and of wavelength results in the two-dimensional plot of transmission shown in Fig. 11. These simulation results are from RCWA using published values for the complex refractive index of silver across the wavelength range simulated.[10] Thousands of individual simulations comprise the 2D plot shown in the figure, transmission was determined at each point as wavelength and film thickness were varied. The film thickness defined here is slightly different from that described in Fig. 3. Film thickness in the vertical plot axis relates to the metal thickness between the two gratings. The grating height is held constant at 60nm for both front and back gratings. Thus, for zero film thickness, there still exists a 120nm grating suspended

in air. This allows us to independently see the effect of the length of the slit from front to back surfaces of the metal.

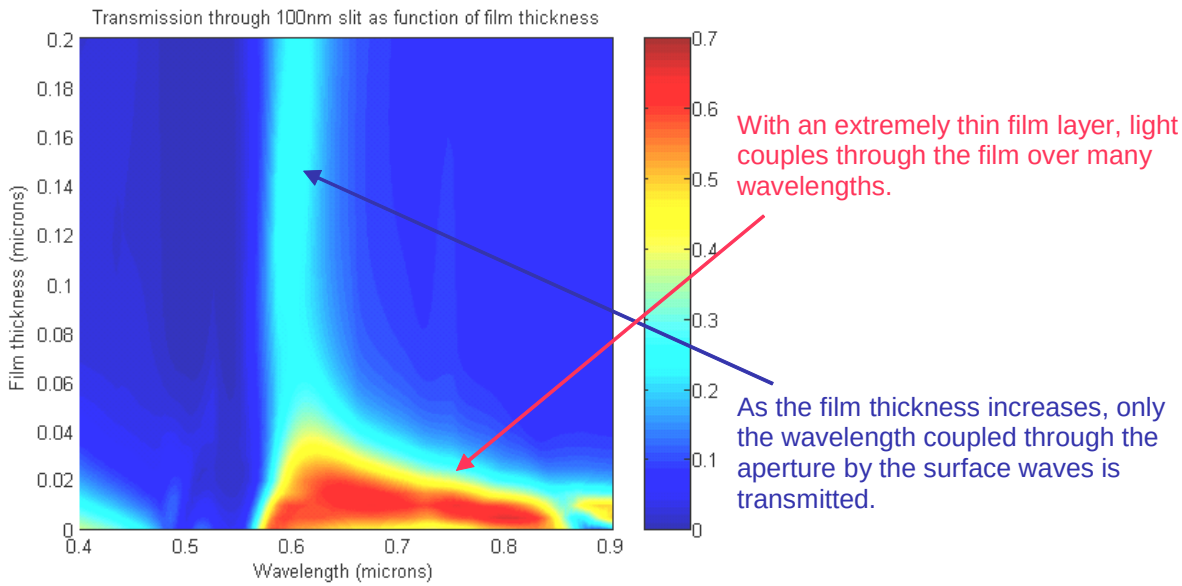

Fig. 11. Transmissivity through a linear aperture in a silver film as a function of wavelength and film thickness.

The results show a strong transmission for very thin metal thicknesses as would be expected. As the metal thickness increases the transmission occurs only at the surface plasmon wavelength and remains relatively constant as a function of thickness. The transmission through the slit does not vary as the film thickness is increased. This result illustrates the ability of the surface plasmon to propagate along the walls of the metal slit, in a manner analogous to a waveguide.

Emission

Emission is another aspect of these surfaces that is intriguing. The absorption into surface plasmon modes also tells us the location of the corresponding emission peaks in the spectra.

The simple plasmon theory predicts well the location of the surface plasmon modes but to calculate the reflection/absorption of the metal surface we utilize the aforementioned transfer matrix method (TMM). In the TMM electromagnetic (EM) waves of fixed frequency impinge on a structure that is periodic in two dimensions but finite in the third direction.

The TMM simulations utilized the frequency-dependent real and imaginary components of the dielectric function of silver for two lattices (Λ = 0.7μm; Λ = 0.5μm). In Fig. 12 and Fig. 13 the transmission, reflection, and absorption are plotted. For a normally incident wave, we find sharp reflectivity dips at the fundamental surface plasmon mode wavelength ($\lambda = \Lambda$), expected from the simple surface plasmon theory (3). The reflectivity falls to almost 0.2 from a long wavelength value of 0.85-0.9, exhibiting an exceedingly narrow full-width half-maximum (FWHM) of 0.1μm , where the incident wave is absorbed by the sharp surface plasmon resonance on the patterned silver film. The narrow FWHM corresponds to $\Delta\lambda/\lambda_0$ = 0.14 and 0.19 for the 0.5μm and 0.7μm lattice constants respectively.

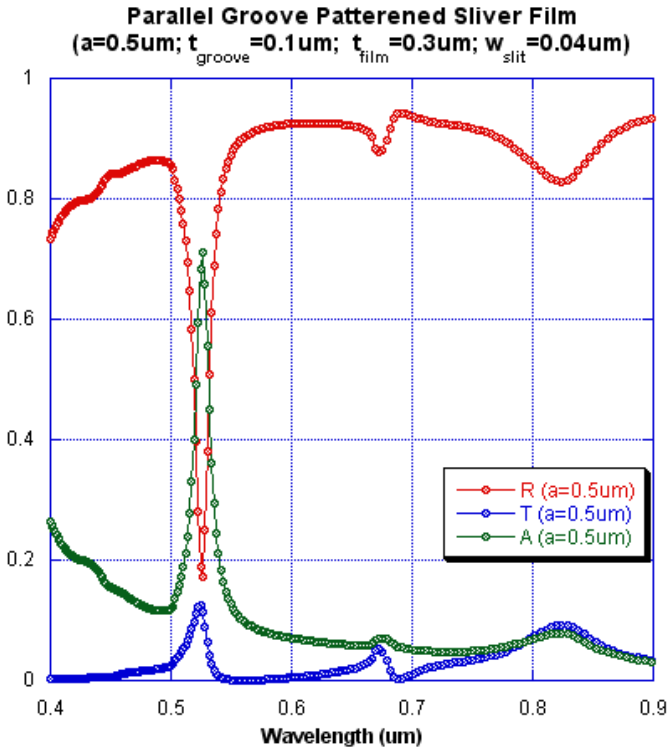

Fig. 12. Reflectivity, transmission, and absorption for parallel apertures in a silver film with a grating period of 0.5μm.

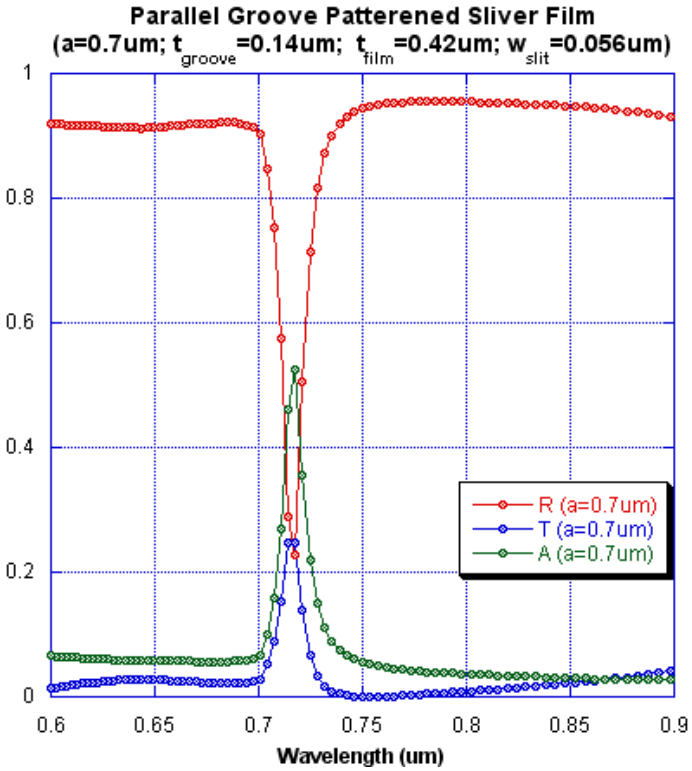

Fig. 13. Reflectivity, transmission, and absorption for parallel apertures in a silver film with a grating period of 0.7μm.

We can thus design a metal surface that is reflective over the spectrum except for a narrow wavelength band where an absorption band can be selectively placed. From an emissivity standpoint, this implies a low emissivity except for a pre-determined band of high emissivity.

Conclusions

We have modeled surface waves at metal-dielectric interfaces and have designed and optimized structures that take advantage of surface plasmon properties. These results could be leveraged in future Sandia projects in areas such as emissivity-control of surfaces, photolithography, near-field microscopy, and biophotonics.

Surface plasmons offer a method for transmission through a tiny aperture without the wide divergence predicted by diffraction theory. We have demonstrated that this divergence is unaffected by changes in the slit width.

We have varied structure parameters such as metal film thickness, grating etch depth, slit width, and period. We have shown that emission and transmission peaks can be spectrally shifted through changes to the period. Transmission through the slit may be optimized with the other parameters.

This project required simulation code development. The resulting code is thus considerably more versatile, and will undoubtedly receive heavy use for modeling future optical structures. A knowledge-base for modeling such structures using RCWA was also developed under this LDRD.

References

[1] T. Thio, H. J. Lezec, T. W. Ebbesen, K. M. Pellerin, G. D. Lewen, A. Nahata, R. A. Linke, “Giant optical transmission of sub-wavelength apertures: physics and applications,” *Nanotechnology*, vol. 13, pp. 429-432, May 2002.

[2] T. W. Ebbesen, H. J. Lezec, H. F. Ghaemi, T. Thio, P. A. Wolff, “Extraordinary optical transmission through subwavelength hole arrays,” Nature, vol. 391, pp. 667-669 (1998)

[3] N. Bonod, S. Enoch, L. Li, E. Popov, M. Nevière , “Resonant optical transmission through thin metallic films with and without holes,” *Opt. Express*, vol. 11, pp. 482-490, 10 March 2003.

[4] H. J. Lezec, A. Degiron,1 E. Devaux,1 R. A. Linke, L. Martin-Moreno, F. J. Garcia-Vidal, T. W. Ebbesen, “Beaming Light from a Subwavelength Aperture,” *Science*, vol. 297, pp. 820-822, 2 Aug. 2002.

[5] M. U. Pralle, N. Moelders, M. P. McNeal, I. Puscasu, A. C. Greenwald, J. T. Daly, E. A. Johnson, T. George, D. S. Choi, I. El-Kady, R. Biswas, “Photonic crystal enhanced narrow-band infrared emitters,” *Appl. Phys. Lett.*, vol. 81, pp. 4685-4687, 16 Dec. 2002.

[6] H. Raether. *Surface Plasmons*, Springer Tracts in Modern Physics Volume 111 (Springer-Verlag 1988).

[7] T. J. Kim, T. Thio, T. W. Ebbesen, D. E. Grupp, H. J. Lezec, Opt. Lett. 24, 256 (1999).

[8] G. R. Hadley, "Numerical simulation of reflecting structures by solution of the two-dimensional Helmholtz equation" , *Opt. Lett*., vol. 19, pp. 84-86, 1993.

[9] G. R. Hadley, “Low-Truncation-Error Finite Difference Representations of the 2-D Helmholtz Equation”, *Int. J. Electron. Commun. (AEU)*, vol. 52, pp. 310-316, 1998.

[10] E. D. Palik, *Handbook of Optical Constants of Solids*, Academic Press, 1985.

Distribution

5	MS 0603	David Peters, 1743
1	MS 0603	Ihab El-Kady, 1743
1	MS 0603	Ron Hadley, 1742
1	MS 0603	Shanalyn Kemme, 1743
1	MS 0972	Chris Lanes, 5721
1	MS 0603	Jim Hudgens, 1743
1	MS 0603	Charles Sullivan, 1742
1	MS 0972	Steve Gentry, 5721
1	MS 0972	Clinton A. Boye, 5710
1	MS 9018	Central Technical Files, 8945-1
1	MS 0123	Donna Chavez, LDRD Office, 1011
2	MS 0899	Technical Library, 9616